

## The Dependency on the Dissipation Tensor of Multi-modal Nuclear Fission

T. Asano,<sup>\*,a,b</sup> T. Wada,<sup>c</sup> M. Ohta<sup>c</sup>, S. Yamaji,<sup>d</sup> and H. Nakahara<sup>e</sup>

<sup>a</sup>Department of Physics, Tohoku University, Sendai, 980-8578, Japan

<sup>b</sup>Laboratory of Nuclear Science, Tohoku University, Mikamine, Sendai 982-0826, Japan

<sup>c</sup>Department of Physics, Konan University, 8-9-1 Okamoto, Kobe 658-8501, Japan

<sup>d</sup>Cyclotron Center, RIKEN, Wako, Saitama 351-0198, Japan

<sup>e</sup>Graduate School of Science, Tokyo Metropolitan University, Tokyo 192-0397, Japan

**Received: January 16, 2006; In Final Form: March 30, 2006**

A multi-dimensional Langevin equation is applied for the study of the multi-modal nuclear fission in actinide region. Two kinds of dissipation tensors, the wall-and-window formula and the wall formula, are used to investigate the dynamical effects of nuclear dissipation. The mass distribution and the total kinetic energy distribution of the fission fragments are calculated for  $^{264}\text{Fm}$  with these dissipation tensors. It is found that the dissipation tensor plays important roles in determining the fission paths. We obtain drastically different mass distributions by applying different models for nuclear friction.

### 1. Introduction

In the study of the fission of actinide nuclei at low excitation energies including the spontaneous fission, it was found that the fragment mass distribution and the total kinetic energy (TKE) distribution consist of more than one component, in contrast to the simple single peak structure that is found in the fission at high excitation energies.<sup>1-6</sup> This phenomenon is attributed to the existence of more than one fission path and is called the multi-modal fission.

The mass and TKE distributions depend sensitively on the excitation energy and the position of the peaks of the mass distribution suggests the influence of the closed shell structure of the fragments. Therefore, it is supposed that the microscopic energy plays an important role for the manifestation of this phenomenon. It is a great challenge for us to understand this phenomenon in terms of nuclear many-body dynamics. Several authors studied the potential energy surface (PES) including the microscopic energy in a multi-dimensional parameter space that describes various nuclear shapes; one can deduce the possible fission paths by studying the location of the saddle points and the fission valleys in multi-dimensional parameter space.<sup>7</sup> With this method, they could explain the general trend of the position of the peaks of the mass distribution.

The dynamical point of view is necessary to progress the study of the fission mode. We have applied the Langevin approach to the study of the fission modes in uranium nuclei and in fermium nuclei.<sup>8-10</sup> We studied the mass and TKE distributions and demonstrated that we can decompose the fission events into several components by tracing the Langevin trajectories. We also studied the isotope dependence and the excitation energy dependence of the fission mode.<sup>8-10</sup> In the previous studies, we adopted the wall-and-window type one-body friction as the dissipation mechanism of the nuclear fission dynamics. The validity of this dissipation mechanism has been demonstrated by one of the authors (T.W.) who studied the dissipation tensor dependence of the pre-scission neutron multiplicity and the mean TKE.<sup>11-14</sup> From the comparison of the results of the dynamical calculation with experimental data, they excluded the possibility of the two-body type dissipation

to be the dominant mechanism by showing that it cannot reproduce the pre-scission neutron data and the TKE data simultaneously. On the other hand, they showed that the wall-and-window type one-body friction can reproduce both data reasonably well and concluded that it is a reasonable model for the dissipation mechanism of nuclear fission.

There are other models that are of one-body nature, e.g. surface-plus-window formula, modified wall-and-window formula and chaos weighted wall formula.<sup>15-17</sup> Though there were no free parameters in the original derivation of the one-body friction,<sup>18, 19</sup> the strength has been modified frequently in order to reproduce some experimental data. For example, in the study of the light particle evaporation and the mass distribution, Schmitt et al. used the strength as a free parameter.<sup>17</sup> The modification itself should be acceptable when we take account of the simplicity of the model; it is a macroscopic model without any microscopic effect and it has no dependence on the temperature. However, when one modifies the strength of the nuclear dissipation just to reproduce only one physical quantity, it might be inappropriate to conclude that the deduced strength has definite physical meanings. It may reflect the other effects completely different from the dissipation, like the insufficiency of the model space. It is very important to compare many (at least more than one) physical quantities at the same time.

Among the physical quantities that are measured in nuclear fission, the TKE and mass distributions are well investigated experimentally in many cases. In this study, we use these quantities to discuss the dissipation dependence of the fission modes. It is shown that the TKE distribution is, as was expected, directly connected to the strength of the dissipation and we can put some constraints on the strength of the dissipation. Furthermore, it is shown that the mass distribution changes rather drastically when one uses different models for the dissipation mechanism. These results demonstrate the importance and the usefulness of the dynamical approach to the study of the fission mode.

Section 2 gives a concise description of our framework. Results are shown in Sec. 3 concerning the fission of  $^{264}\text{Fm}$  nucleus at  $E_x = 20$  MeV. Summary is given in Sec. 4.

### 2. Methods

In this study, a multi-dimensional Langevin equation is used

\*Corresponding author. E-mail: mail: asano@nucl.phys.tohoku.ac.jp

to demonstrate the dynamics of multi-modal fission. It has been successfully applied to the study of nuclear dynamics of fission and fusion-fission.<sup>8-17, 20-23</sup> The time evolution of the fission process in the multi-dimensional deformation space is traced starting from the ground state of the fissioning nucleus via saddle points to various scission configurations.

The multi-dimensional Langevin equation has the following form;

$$\frac{dq_i}{dt} = (m^{-1})_{ij} p_j,$$

$$\frac{dp_i}{dt} = -\frac{\partial V}{\partial q_i} - \frac{1}{2} \frac{\partial}{\partial q_i} (m^{-1})_{jk} p_j p_k - \gamma_{ij} (m^{-1})_{jk} p_k + g_{ij} R_j(t),$$

where the  $q_i$  denote collective coordinates in the deformation space and the  $p_i$  are the conjugate momenta. The summation from 1 to  $n$  over the repeated indices is assumed with  $n$  being the number of collective degrees of freedom. In this study, we use the distance between the centers of mass of the two future fragments  $R_{CM}$ , the fragment deformation parameter  $\delta$  and the mass-number of one fragment  $A_1$  as three collective variables to describe the dynamics of the multi-modal fission.  $V(q)$  is the potential energy and  $m_{ij}(q)$  and  $\gamma_{ij}(q)$  are the shape-dependent collective inertia and dissipation tensors, respectively. The normalized random force  $R_i(t)$  is assumed to be a white noise, i.e.,  $\langle R_i(t) \rangle = 0$ ,  $\langle R_i(t_1) R_j(t_2) \rangle = 2\delta_{ij} \delta(t_1 - t_2)$ . The strength of the random force  $g_{ij}$  is given by  $\sum_k g_{ik} g_{jk} = T\gamma_{ij}$ , where  $T$  is the temperature of the compound nucleus. The hydrodynamical inertia tensor is calculated by means of the Werner-Wheeler approximation for the velocity field.<sup>24</sup>

Two types of the dissipation tensors are used in this study, namely the wall-and-window formula and the wall-formula.<sup>18, 19</sup> Both are the so called one-body friction and the difference lays in their behavior when the system has a developed neck. Figures 1, 2, and 3 show the diagonal components of the two dissipation tensors. Results are shown for the mass-symmetric fission of  $^{264}\text{Fm}$  with  $\delta = 0.0$ . Figure 1 shows the diagonal component  $\gamma_{RR}$  as a function of  $R_{CM}$ . It is seen that the wall-and-window formula gives a smaller  $\gamma_{RR}$  at the saddle region ( $0.5 < R_{CM} < 0.7$ ). It stays smaller than the wall formulae value toward the scission region. Figure 2 shows the diagonal component  $\gamma_{\delta\delta}$ . Both formulae give essentially the same results. A remarkable difference is seen in Figure 3 that shows the diagonal component  $\gamma_{AA}$ . The friction for the mass-asymmetric degree of freedom becomes infinitely large in the wall-and-window formula as the neck radius vanishes. As we will see later, this special feature gives us a very distinct difference in the fragment mass distribution. We also modify the strength of the dissipation by introducing the strength parameter  $k_s$ ;

$$\gamma_{ij}^{\text{wall-and-window}}(k_s) = k_s \gamma_{ij}^{\text{wall-and-window}},$$

$$\gamma_{ij}^{\text{wall}}(k_s) = k_s \gamma_{ij}^{\text{wall}}.$$

We take the following values for  $k_s$  in this study;  $k_s = 1.0, 0.5$ , and  $0.25$  for the wall-and-window formula (WWF) and  $k_s = 1.0$  and  $0.25$  for the wall formula (WF).

Since it is essential for this study to take account of the microscopic energy, the potential energy is calculated using the macroscopic-microscopic method. We use TWOCSTR of two-center shell model code to calculate the potential energy surface.<sup>25-27</sup> The origin of the potential energy is set so that the macroscopic energy for the spherical shape vanishes. We do not take account of the effect of the angular momentum or the particle evaporation in this study. Those who are interested in the numerical procedure should read References 8 and 10 and the references therein.

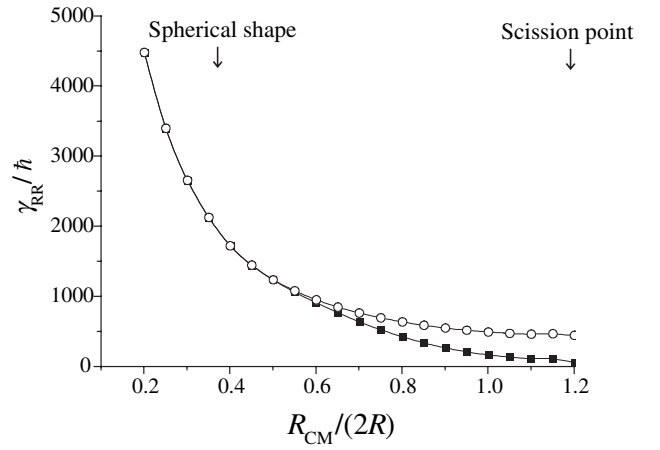


**Figure 1.** The diagonal component  $\gamma_{RR}$  of the dissipation tensor with  $\delta=0.0$  for the mass-symmetric fission of  $^{264}\text{Fm}$  calculated with the wall-and-window formula (solid squares) and with the wall formula (open circles). The abscissa denotes the distance between the centers of mass of future fission fragments.  $R$  is the radius of the parent nucleus. In both cases, the strength parameter is set to unity.

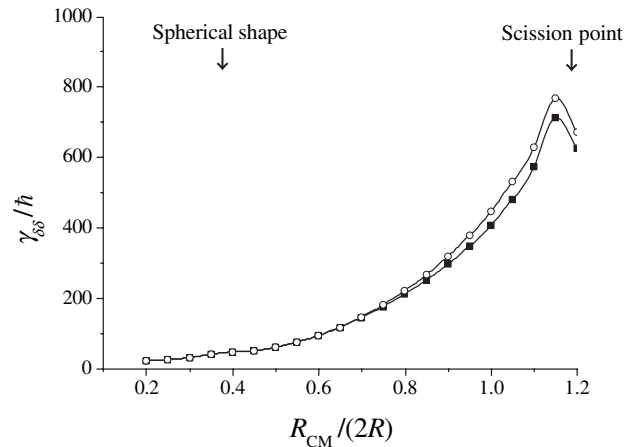


**Figure 2.** The diagonal component  $\gamma_{\delta\delta}$  of the dissipation tensor with  $\delta=0.0$  for the mass-symmetric fission of  $^{264}\text{Fm}$ . The meaning of each symbol is the same as that in Figure 1.

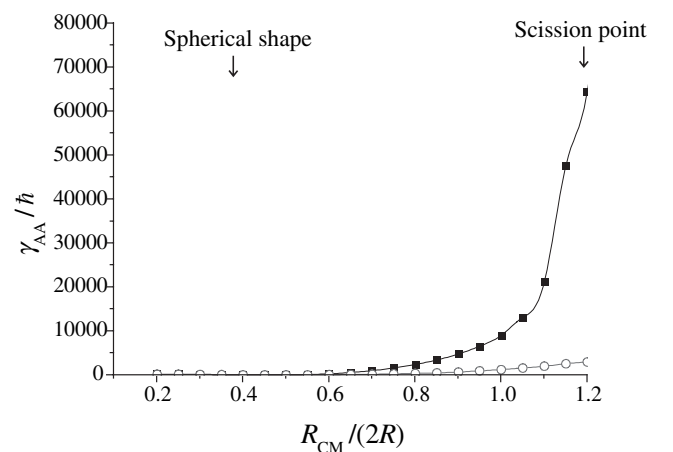


**Figure 3.** The diagonal component  $\gamma_{AA}$  of the dissipation tensor with  $\delta=0.0$  for the mass-symmetric fission of  $^{264}\text{Fm}$ . The meaning of each symbol is the same as that in Figure 1.

### 3. Results

As an example, we calculate the fission of  $^{264}\text{Fm}$  at the excitation energy  $E_x = 20.0$  MeV.  $^{264}\text{Fm}$  has a special feature; it is divided into two identical doubly-magic fragments  $^{132}\text{Sn}$  ( $Z=50, N=82$ ). Though there are no fission experiments available for this nucleus, we chose it for our calculation

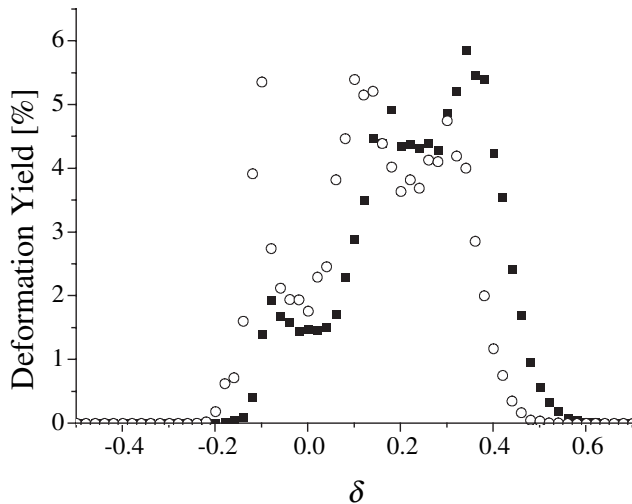


**Figure 4.** Distribution of the deformation parameter  $\delta$  at the scission configuration for the fission of  $^{264}\text{Fm}$  at  $E_x = 20.0$  MeV. Solid squares denote the results with the wall-and-window formula ( $k_s = 1.0$ ) and open circles the results with the wall formula ( $k_s = 0.25$ ). The sum over the distribution is normalized to 100%.

**TABLE 1: Peak values of the mass number of one fragment,  $\langle A_1 \rangle$ , and that of the TKE,  $\langle \text{TKE} \rangle$ , obtained from the Gaussian fitting to each component and the shape elongation  $\beta$  deduced from  $\langle A_1 \rangle$  and  $\langle \text{TKE} \rangle$ .**

Dissipation formula	$k_s^*$	Fission mode	$\langle A_1 \rangle$	$\langle \text{TKE} \rangle$ (MeV)	$\beta$	
Wall-and-window	1.00	Component I	131.7	230.6	1.32	
		Component II	142.5	203.9	1.49	
		Component III	131.1	181.7	1.68	
	0.50	Component I	131.5	237.8	1.28	
		Component II	143.4	212.6	1.42	
		Component III	131.4	190.5	1.60	
		0.25	Component I	131.4	244.1	1.25
			Component II	142.9	220.1	1.38
			Component III	131.1	200.0	1.52
Wall	1.00	Component I	131.5	222.3	1.37	
		Component II	137.9	196.1	1.55	
		Component III	131.5	175.5	1.74	
	0.25	Component I	131.5	234.9	1.30	
		Component II	139.0	210.3	1.45	
		Component III	131.4	192.1	1.59	

\*The second column represents the strength parameter  $k_s$ .

because of this special feature. We perform the dynamical calculations with WWF dissipation and also with WF dissipation.

In the previous study of the fission of  $^{264}\text{Fm}$ , we showed that we can classify the fission events by using the value of the deformation parameter  $\delta$  at scission configuration.<sup>8</sup> Figure 4 shows the distribution of the deformation parameter  $\delta$  at scission configuration. In the figure, solid squares express the results with WWF with  $k_s = 1.0$  and open circles express the ones with WF with  $k_s = 0.25$ . These values of the strength parameter  $k_s$  are recommended in the earlier studies of the mean total kinetic energies of the fragments.<sup>28</sup> In Figure 4, we can clearly see the three-peak structure both in WWF case and in WF case. For example, we decompose the fission events in the case of WWF with  $k_s = 1.0$  into three components according to the value of  $\delta$  at scission configuration: Component I ( $\delta < 0.0$ ), Component II ( $0.0 < \delta < 0.24$ ), and Component III ( $\delta > 0.24$ ). Similar decomposition is made for other cases with different strength parameter  $k_s$  and with different dissipation formula. In general, smaller value of  $\delta$  means larger value of TKE because of the compactness of the scission configuration.

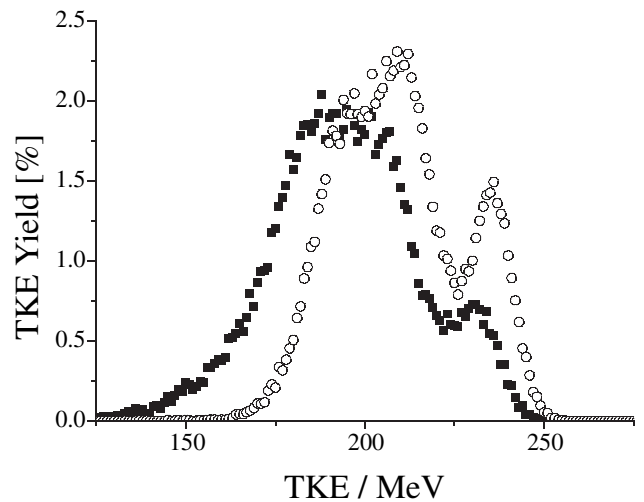


**Figure 5.** Distribution of the TKE for the fission of  $^{264}\text{Fm}$  at  $E_x = 20.0$  MeV. The meaning of each symbol is the same as that in Figure 4.

It was also found in the previous study that Components I and III correspond to the mass-symmetric fission and Component II to the mass-asymmetric fission.<sup>8</sup>

Table 1 shows the summary of the calculation with various dissipation tensors. Results are given for the peak value of the TKE,  $\langle \text{TKE} \rangle$ , that of the fragment mass number,  $\langle A_1 \rangle$ , and the shape elongation  $\beta$  for each of the three modes. The values for  $\langle \text{TKE} \rangle$  and  $\langle A_1 \rangle$  are obtained with the Gaussian fitting of the distributions. The shape elongation  $\beta$  was introduced by Zhao et al. in their systematic study of the TKE in the actinide region.<sup>29,30</sup> They assumed that the TKE is equal to the Coulomb energy between point charges at the scission configuration and they deduced the separation of the point charges  $D$  from the observed TKE, namely  $\text{TKE} = Z_1 Z_2 e^2 / D$ . Then they defined the shape elongation at the scission point  $\beta = D / (R_1 + R_2)$ , where the denominator  $R_1 + R_2$  is the distance between the charge centers of two touching spherical fragments. They showed that there are mainly two types of scission configurations; a mass-asymmetric ( $A_H = 140$ ) configuration with  $\beta = 1.53$  and a mass-symmetric configuration with  $\beta = 1.65$ . They also showed that the value of  $\beta$  for each mode is almost independent of the mass number of the fissioning nucleus. For the nucleus whose mass number is nearly equal to 260, there is an additional mass-symmetric compact configuration with  $\beta = 1.33$ . Since those values of  $\beta$  do not vary much with the change of the proton and the neutron numbers,<sup>29,30</sup> we assume those values are also applicable to  $^{264}\text{Fm}$ . One easily sees from Table 1 that Component I corresponds to the mass-symmetric compact configuration, Component II corresponds to the mass-asymmetric configuration, and Component III corresponds to the mass-symmetric elongated configuration. By comparing the values of  $\beta$  in Table 1 with the systematic values, we can confirm the validity of the suggested value of  $k_s$  in the sense that  $\langle \text{TKE} \rangle$  is reproduced well. It is clearly seen that  $\langle \text{TKE} \rangle$  changes significantly and becomes larger for all components when we use a smaller value of  $k_s$ , that means weaker one-body friction. Thus it is inappropriate to deduce the value of  $k_s$  from other physical quantities without taking account of its effect on the mean TKE.

Next, we compare the results of WWF with that of WF more in detail. Figure 5 shows the TKE distribution for the same system as that in Figure 4. Again, solid squares denote the results with WWF ( $k_s = 1.0$ ) and open circles denote the ones with WF ( $k_s = 0.25$ ). It is clearly seen that by using the different types of dissipation tensors, we obtain a different fraction of contribution from each mode. It should be noted that we do not obtain this kind of change in the fraction of contribution from each mode when we only change the strength

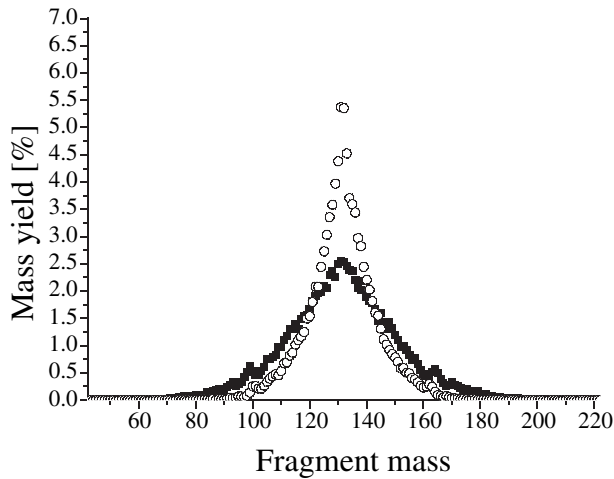


**Figure 6.** Distribution of the fragment mass number for the fission of  $^{264}\text{Fm}$  at  $E_x = 20.0$  MeV. The meaning of each symbol is the same as that in Figure 4.

parameter  $k_s$  within the same dissipation formula. The contribution of Component I, the compact mass-symmetric component that has the largest TKE, is much larger in WF case than that in WWF case. It should also be noted that we use the same potential energy surface in both calculations, that means the barrier height for Component I mode is the same in both cases. Therefore, we can say that the difference of the contribution comes solely as a dynamical effect on the motion from saddle region to scission configuration. In Figure 6, we show the fragment mass distribution for the same system. It is seen that the contribution from the mass-symmetric mode (Component I) is much larger in the case of WF which is consistent with the previous result. As a result, the mass distribution is much sharper for WF than that for WWF. Thus in principle, we can determine which model is more appropriate for the description of the phenomenon of multi-modal fission by comparing the contribution from each mode with experiments. This fraction of the contribution is, of course, very sensitive to the height of the fission barrier for each mode. So it is necessary to obtain a reliable microscopic energy surface before we draw a definite conclusion about the model for the nuclear dissipation.

In order to see the origin of the huge difference in the two models for the dissipation, we calculate the fission trajectory without the random force starting from several points in the saddle region. We take the starting points at  $R_{\text{CM}}/(2R) = 0.7$  with  $\delta = -0.1, 0.0, 0.1, 0.13, 0.2$ , and  $0.3$ . The initial mass asymmetry is taken as zero in all cases. Figure 7 shows the results of the calculation without the random force. It is easily seen that even when we start from the same initial point, the final scission configuration varies depending on the model for the dissipation. WWF prefers more elongated shapes than WF does. Because of this tendency, it is expected that WF has larger contribution from compact scission configuration, i.e. WF has larger contribution from Component I.

This dissipation tensor dependence comes from the difference in the structure of the dissipation tensors of these two models. A significant difference is seen in the diagonal component  $\gamma_{\text{AA}}$  (Figure 3). Concerning the mass transfer, both dissipation tensors have the same tendency starting from the ground state shape up to the saddle region ( $R_{\text{CM}}/(2R) = 0.7$ ), however, after passing this region the two dissipation models show completely different aspects. The component  $\gamma_{\text{AA}}$  of WWF increases inversely proportional to the area of the window between the fragments, thus it is very difficult for the system to change its mass-asymmetry after it passes the saddle region when the system has a developed neck. In Reference 8, we studied the potential energy surface of this system in order to study the origin the fission modes. The lowest fission saddle

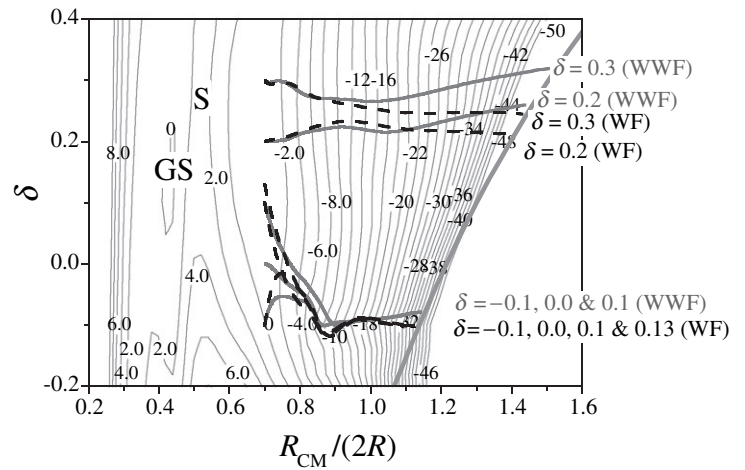


**Figure 7.** The contour plot of the PES for the mass-symmetric fission of  $^{264}\text{Fm}$ . The abscissa denotes the distance between the centers of mass of future fission fragments and the ordinate the deformation parameter  $\delta$ .  $R$  is the radius of the parent nucleus. The ground state and the saddle point are marked by GS and S, respectively. Thick solid lines and dashed lines show the dynamical trajectories without the random force starting from several points in the saddle region:  $R_{\text{CM}}/2R = 0.7$  and  $\delta = -0.1, 0.0, 0.1, 0.13(\text{WF}), 0.2$  and  $0.3$ , respectively. Thick solid lines denote the results with the wall-and-window formula ( $k_s = 1.0$ ) and dashed lines the results with the wall formula ( $k_s = 0.25$ ).

(second saddle) lies at a finite mass-asymmetry, the mass-asymmetry increases first from the ground state to the saddle point. But then in this system, there is a deep mass-symmetric fission valley after the saddle region and the mass-asymmetry tends to decrease toward the symmetric fission valley. In the case of WF, this mechanism works after the saddle region and enhances the contribution of Component I. On the other hand, in the case of WWF, the strong dissipation in mass-asymmetric degree of freedom prevents the system to change its mass-asymmetry.

#### 4. Summary

We have investigated the dissipation dependence of the multi-modal nuclear fission in actinide region. We have used the wall-and-window and the window formula to derive the dissipation tensor and have modified the strength with an overall factor. We have calculated the TKE and fragment mass distributions for the fission of  $^{264}\text{Fm}$  at  $E_x = 20.0$  MeV with these dissipation tensors. By comparing the results with different dissipation tensors, we found that the dissipation tensor affects not only the TKE distribution but also the fragment mass distribution through the change in the contribution of each fission mode. Although the multi-modal fission phenomenon is often discussed from the static point of view by using the potential energy surface, we have shown that the dynamical effects of the dissipation tensor play essential roles in determining the TKE and mass distributions. The TKE distribution is very sensitive to the strength of the dissipation, while distinct mass distributions are obtained when we adopt different dissipation models. From the comparison with the systematics of the experimental shape elongation  $\beta$ , we suggest that the wall-and-window formula with  $k_s = 1.0$  can be a reasonable model for the dissipation in fission phenomena. It is desirable to extend the model space to be able to compare the calculated mass distribution with experiments more quantitatively. We also plan to adopt the microscopic inertia and dissipation tensors that are based on the linear response theory.<sup>27,31</sup>

**Acknowledgements.** The authors wish to express their gratitude to Dr. T. Ichikawa, Dr. Y. Nagame, Prof. Y. L. Zhao,

Prof. N. Takigawa, Prof. K. Hagino, and Prof. F. Hanappe for their useful discussions. One of the authors (T. W.) is partially supported by a Grant-in-Aid for Scientific Research No. 17540270 provided by the Japan Society for the Promotion of Science.

## References

- (1) R. C. Ragaini, E. K. Hulet, R. W. Lougheed, and J. Wild, *Phys. Rev. C* **9**, 399 (1974).
- (2) W. John, E. K. Hulet, R. W. Lougheed, and J. J. Wesolowski, *Phys. Rev. Lett.* **27**, 45 (1971).
- (3) J. P. Balagna, G. P. Ford, D. C. Hoffman, and J. D. Knight, *Phys. Rev. Lett.* **26**, 145 (1971).
- (4) E. K. Hulet, J. F. Wild, R. J. Dougan, R. W. Lougheed, J. H. Landrum, A. D. Dougan, M. Schädel, R. L. Hahn, P. A. Baisden, C. M. Henderson, R. J. Dupzyk, K. Sümmerer, and G. R. Bethune, *Phys. Rev. Lett.* **56**, 313 (1986).
- (5) E. K. Hulet, J. W. Wild, R. J. Dougan, R. W. Lougheed, J. H. Landrum, A. D. Dougan, P. A. Baisden, C. M. Henderson, and R. J. Dupzyk, *Phys. Rev. C* **40**, 770 (1989).
- (6) H. C. Britt, D. C. Hoffman, J. van der Plicht, J. B. Wilhelmy, E. Cheifetz, R. J. Dupzyk, and R. W. Lougheed, *Phys. Rev. C* **30**, 559 (1984).
- (7) P. Möller, D. G. Madland, A. J. Sierk, and A. Iwamoto, *Nature* **409**, 785 (2001).
- (8) T. Asano, T. Ichikawa, T. Wada, M. Ohta, S. Yamaji, and H. Nakahara, *J. Nucl. and Radiochem. Sci.* **5**, 1 (2004).
- (9) T. Asano, T. Ichikawa, T. Wada, M. Ohta, S. Yamaji, and H. Nakahara, *Prog. Theor. Phys. Suppl.* **154**, 457 (2004).
- (10) T. Asano, Doctoral thesis. Konan University (2004).
- (11) T. Wada, N. Carjan, and Y. Abe, *Nucl. Phys. A* **538**, 283c (1992).
- (12) T. Wada, Y. Abe, and N. Carjan, *Phys. Rev. Lett.* **70**, 3538 (1993).
- (13) T. Wada, *Proc. the Second Tours Sympo. on Nuclear Physics*, ed. by H. Utsunomiya, M. Ohta, J. Galin, and G. Münzenberg (World Scientific, Singapore, 1995), p470.
- (14) Y. Abe, S. Ayik, P. –G. Reinhard, and E. Suraud, *Phys. Rep.* **275**, 49 (1996).
- (15) A. V. Karpov, P. N. Nadtochy, D. V. Vanin, and G. D. Adeev, *Phys. Rev. C* **63**, 054610 (2001).
- (16) G. Chaudhuri and S. Pal, *Phys. Rev. C* **63**, 064603 (2001).
- (17) C. Schmitt, J. Bartel, K. Pomorski, and A. Surowiec, *Acta Phys. Pol.* **B34**, 1651 (2003).
- (18) J. Blocki, Y. Boneh, J. R. Nix, J. Randrup, M. Robel, A. J. Sierk, and W. J. Swiatecki, *Ann. Phys.* **113**, 330 (1978).
- (19) J. Randrup and W. J. Swiatecki, *Nucl. Phys. A* **429**, 105 (1984).
- (20) T. Ichikawa, Doctoral thesis. Konan University (2003).
- (21) Y. Aritomo and M. Ohta, *Nucl. Phys. A* **744**, 3 (2004).
- (22) P. Fröbrich and I. I. Gontchar, *Phys. Rep.* **292**, 131 (1998).
- (23) A. V. Karpov, P. N. Nadtochy, E. G. Ryabov, and G. D. Adeev, *J. Phys. G* **29**, 2365 (2003).
- (24) K. T. R. Davis, A. J. Sierk, and J. R. Nix, *Phys. Rev. C* **13**, 2385 (1976).
- (25) S. Suekane, A. Iwamoto, S. Yamaji, and K. Harada, JAERI-memo 5918 (1974).
- (26) A. Iwamoto, S. Yamaji, S. Suekane, and K. Harada, *Prog. Theor. Phys.* **55**, 115 (1976).
- (27) K. Sato, S. Yamaji, K. Harada, and S. Yoshida, *Z. Phys. A* **290**, 149 (1979).
- (28) J. R. Nix and A. Sierk, LA-UR-86-698 (1986).
- (29) Y. L. Zhao, Y. Nagame, M. Tanikawa, K. Tsukada, S. Ichikawa, K. Sueki, Y. Oura, H. Ikezoe, S. Mitsuoka, H. Kudo, and H. Nakahara, *Phys. Rev. Lett.* **82**, 3408 (1999).
- (30) Y. L. Zhao, Y. Nagame, I. Nishinaka, K. Sueki, and H. Nakahara, *Phys. Rev. C* **62**, 014612 (2000).
- (31) H. Hofmann, *Phys. Rep.* **284**, 137 (1997).